

Article

An In Vivo Evaluation of Biocompatibility and Implant Accuracy of the Electron Beam Melting and Commercial Reconstruction Plates

Khaja Moiduddin ^{1,*}, Syed Hammad Mian ¹, Mohammed Alkindi ², Sundar Ramalingam ², Hisham Alkhalefah ¹ and Osama Alghamdi ²

¹ Advanced Manufacturing Institute, King Saud University, Riyadh 11421, Saudi Arabia; syedhammad68@yahoo.co.in (S.H.M.); halkhalefah@ksu.edu.sa (H.A.)

² Department of Oral and Maxillofacial Surgery, College of Dentistry, King Saud University, Riyadh 11545, Saudi Arabia; malkindi@ksu.edu.sa (M.A.); smunusamy@ksu.edu.sa (S.R.); oghamdi@ksu.edu.sa (O.A.)

* Correspondence: kmoiduddin@gmail.com or khussain1@ksu.edu.sa; Tel.: +096-611-469-7372

Received: 2 September 2019; Accepted: 26 September 2019; Published: 30 September 2019



Abstract: The use of additive manufacturing in medical applications has become more prevalent over the last decade. Studies have proved that reconstruction plates with a mesh structure enhance the biocompatibility and bone-ingrowth formation. However, limited studies have been reported in the customization and in vivo clinical assessment of mesh implants. The purpose of this study was to investigate the surgical treatment and implant fitting accuracy using three different reconstruction plates. Fifteen goats were divided into one control and three experimental groups (Groups 1, 2, and 3) with five in each group. An experimental segmental defect was created on these animals and was adopted with customized electron beam melting reconstruction titanium plates with mesh in Group 1 and without mesh in Group 2 and commercial reconstruction plate in Group 3. All the animals were subjected to radiographic analysis before and after surgery. The subjected animals were sacrificed after 3 months and the electron beam melting reconstruction plates were compared with the commercial plate based on clinical and histology analysis and implant fitting accuracy. Both the electron beam melting reconstruction plates (with mesh and without mesh) and commercial plates survived the three months post-operation, revealing good wound-healing with new bone formation and without any foreign-body reaction. The electron beam melting reconstructed plate with mesh (Group 1) was found to have a better implant fitting when compared to the other two groups. The average discrepancy between Groups 2 and 3 was not significant. Certainly, the commercial plate (Group 3) was found to have the least accuracy as compared to other electron beam melting reconstruction plates (Group 1 and Group 2). Custom design electron beam melting fabricated reconstruction plates possessed better functionality, aesthetic outcome, and long-term biocompatibility when compared to commercial plates. Animal results indicated that the electron beam melting plates with mesh (Group 1) were superior in comparison to the other two groups due to its ability to provide better bone-in-growth and osseointegration on its porous microstructure.

Keywords: electron beam melting; reconstruction plates; 3D comparison; implant fitting accuracy; commercial plate; titanium alloy

1. Introduction

Reconstruction of mandibular deficiencies poses a serious challenge for maxillofacial surgeons due to its unique anatomy and diversity of defects. Any disruption in mandibular continuity leads to functional deformities and severely affects patient self-perception and confidence [1]. Restoring

bony continuity alone should not be seen as a measure of success, but the functionality of oral, chewing, speech articulation, and aesthetic and facial form must also be addressed. The primary goal of mandibular reconstruction is to restore patient functionality to its previous state which in turn can support aesthetic rehabilitation and occlusion, and improve the quality of life post-operation. Paramount to a successful mandibular reconstruction is accurate fitting of the plate onto the bone contours and maintaining the occlusion status of the patient.

In this research study, two titanium reconstruction plates, one with mesh and one without mesh were custom-designed from a pre-operative computed tomography (CT) scan. The selection of titanium alloy for medical implementation is due to its unique combination of high strength-to-weight ratio, low density, superior biocompatibility, high chemical stability, excellent corrosion resistance, and good mechanical properties [2]. The custom-designed reconstruction plates were fabricated using electron beam melting (EBM) additive manufacturing technology and clinically implanted in goats. The use of EBM has revolutionized the way the restoration of complex deficiencies of maxillofacial skeletons is planned. EBM technology can produce complex parts in a layer-by-layer fashion based on computer-aided design (CAD) obtained from a patient CT scan. Due to recent advancements in image processing, EBM technology has facilitated the custom design of complex functional parts based on scanned image data, such as CT and magnetic resonance imaging (MRI). Published literature demonstrates the suitability of EBM-produced titanium implants in biomedical and clinical applications [3,4]. EBM-fabricated mesh implants provide good osteoconductive properties and promote full bone-ingrowth when compared to bulk parts [5,6]. The rapid translation of laboratory findings to clinical application has resulted in a major shift towards large animals whose anatomy and physiology correlate with human physiology. Research and preclinical trials suggest that the TMJ (temporo-mandibular joint) of sheep and goats are anatomically similar to that of humans [7,8].

The EBM-fabricated customized plates of mesh and without mesh was compared with commercially available titanium implants clinically. The customized EBM reconstruction plates are similar to the commercial plates except that instead of manually bending them to match the bone contours, they are fabricated in the proper bend fashion matching the bony contours. Subsequently, the strength and lifespan of the commercial reconstruction plates diminish due to the frequent bending and twisting of the plate to match the bone contours [9]. Moreover, bony reconstruction with commercial plates is both time-consuming and expensive as the surgeons must manually bend and match the plate during surgery [10,11]. Therefore, there is a real need for reconstruction strategy that meets both the aesthetic and functional requirements of the patient and is easy and straightforward for the surgeons in terms of surgery and should achieve a longer implant lifespan with long-term success. Some of the stated advantages of EBM-produced reconstruction plates are accurate fitting, aesthetic restoration, faster healing, better patient occlusion status post-operatively, and shorter operative time [12]. Custom-designed plates result in an increase of interface area between the bone and plate which in effect diminishes the mechanical stresses and consequently allows the reduction of the plate thickness. Recently, several studies have demonstrated the EBM viability of custom-designed implants using an *in vivo* study [13,14]; nevertheless, there have been very few investigations on the biocompatibility comparison of custom-designed EBM-fabricated plates with a commercial plate using an *in vivo* study.

EBM-produced titanium (Ti6Al4V ELI) parts have previously been implanted in several animal and human studies because of their high strength to low weight ratio and corrosion resistance [15,16]. Ti6Al4V ELI (extra-low interstitial, ASTM grade 23) is very similar to Ti6Al4V, except that it provides improved ductility and fracture toughness [17]. However, very few studies have been reported in the customization and *in vivo* clinical assessment of mesh implants. This research study aimed to determine the outcome of the surgical treatment of three different reconstruction plates in comparison with the fitting accuracy and clinical outcomes.

2. Methodology

The flowchart in Figure 1 represents the research methodology comprising various stages and the interface between clinicians and engineers. The interface acts as a communication link to analyze and access the various aspects starting from the patient CT scan to final clinical analysis. The communication interface helps in improving the implant design, reducing clinical errors, and providing satisfaction to the patient.

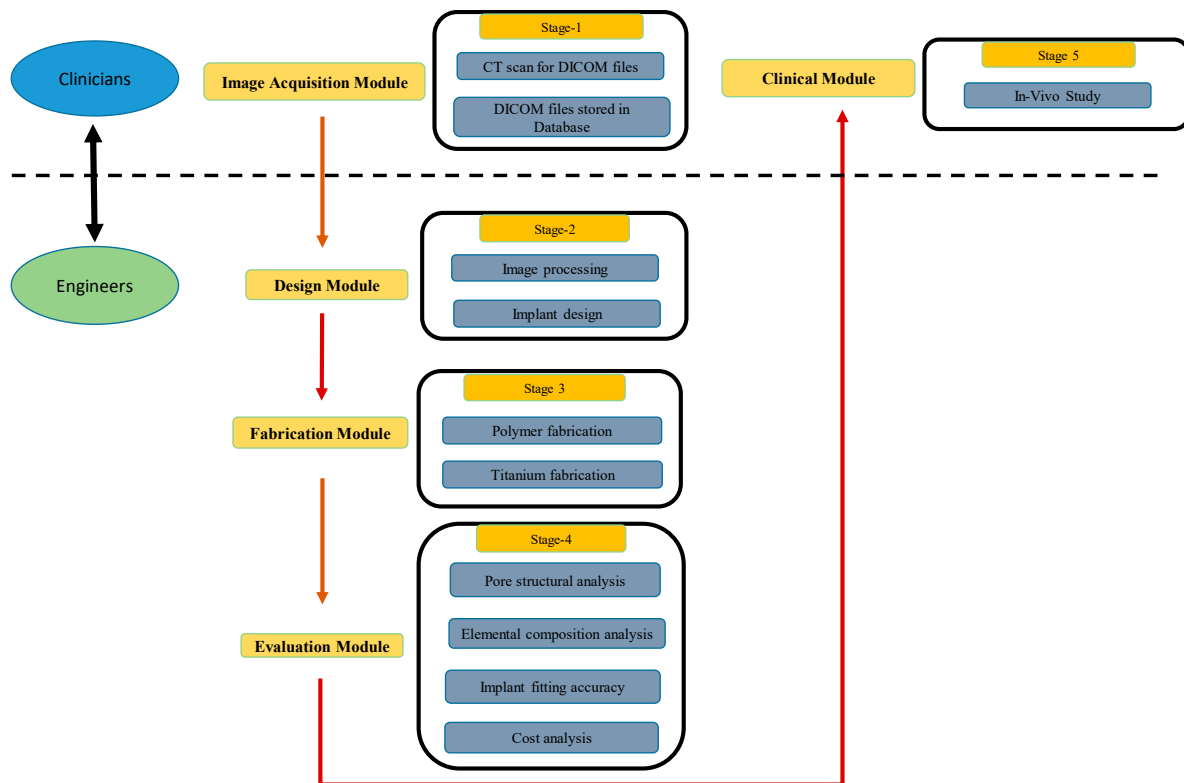


Figure 1. Research methodology for qualified implant consisting of five modules.

Because of the anatomical and physiological similarities to humans, the goat is a common animal model used for clinical research [7]. Following institutional ethics committee approval (College of Dentistry Research Center, King Saud University, Riyadh, Saudi Arabia (Registration # PR-0034)) in conformity with the NIH guidelines (NIH Publication # 85-23 Rev.1985), a group of fifteen ($n = 15$) healthy male goats were selected with an approximate age of 18 months and a weight of 24–28 kg. All the animals were housed under veterinary care in the animal housing laboratory of our institution and were monitored for 2 weeks before surgery. All the animals were vaccinated for common illnesses and were free from any lesions. They were provided with adequate access to food and water throughout the experiment process.

2.1. Image Processing and Implant Design

The animals were subjected to CT under general anesthesia, and the acquired CT scan images were stored as DICOM (Digital Imaging and Communication in Medicine). A DICOM file is a standardized way of storing and transmitting medical images. A ProMax 3D CBCT (cone beam computed tomography) machine (Helsinki, Finland) was used for CT scan (Figure 2a) and the obtained DICOM images were stored in a database (Figure 2b). The acquired scan images were imported into medical processing software known as Mimics® 17.0 (Materialise NV, Leuven, Belgium). Mimics® processes the 2D DICOM images (Figure 2c) and creates a 3D surface model as shown in Figure 2d. Region-growing and segmentation techniques were employed in Mimics® to partition into different

regions (Figure 2e) until the region of interest (mandible) was achieved (Figure 2f). The next step was to design the implant, taking mandible as the template. An outer region of the mandible was marked (Figure 2g) in the shape of an implant and extracted (Figure 2h) which acted as an outline pattern for implant design. An offset thickness of 2 mm (Figure 2i) was provided and the inner region was sectioned (Figure 2j) to replace the bulk part with porous.

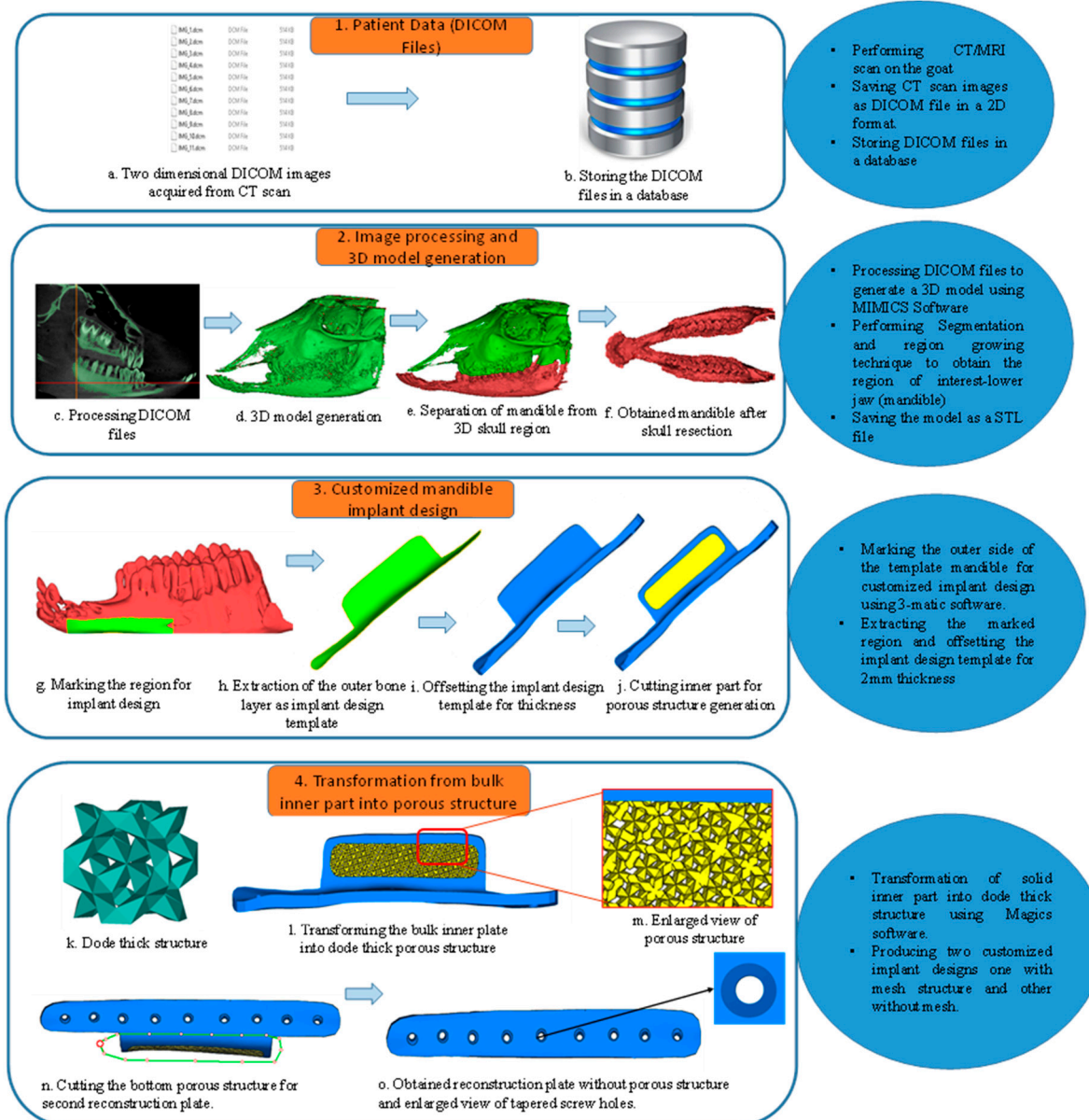


Figure 2. Customized goat implant design steps from DICOM files.

The implant design file was imported into Magics 18.0 (Materialise, NV, Leuven, Belgium) and a porous design cell type of dode thick structure (Figure 2k) was patterned in the middle solid region (Figure 2l) to transform the bulk to porous to get the first reconstruction plate with mesh. A second reconstruction plate (Figure 2o) was constructed by removing the bottom porous part (Figure 2n). The difference between the two plates was that the prior design plate was porous in the middle region where the latter plate has no porous structure. The aim of reconstructing two implant plates was to analyze the effect of porosity with respect to another.

The two designed reconstruction plates of STL (Standard Tessellation Language) files were virtually assembled and aligned with the goat mandible for fitting and rehearsal purposes. A small

mandibular section (colored green) was resected (Figure 3a,c) and a customized porous plate was assembled (Figure 3b,d,e) to verify the design. Similarly, the plate without porous structure was also analyzed (Figure 3f) and was found to be in an exact fit without any deviation from the mandible region. Both reconstruction plates aligned well with the mandibular bone, thus satisfying the assembly and rehearsal evaluation.

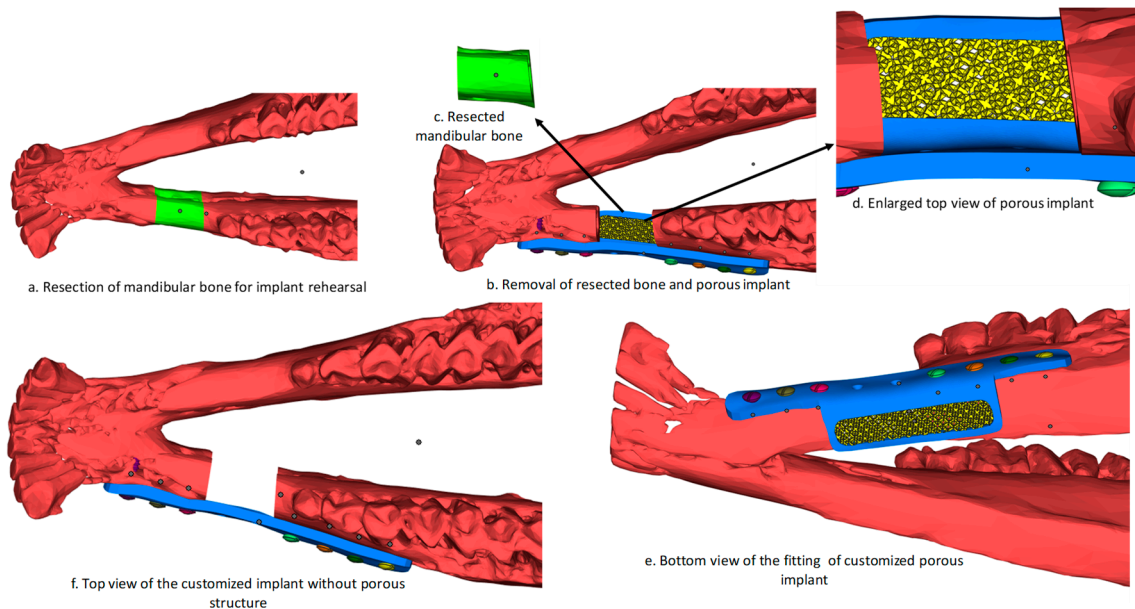


Figure 3. Virtual representation of mandibular bone resection and fitting of customized mandibular plates.

2.2. 3D Printing Reconstruction Plates

Upon successful virtual rehearsal and fitting operation, the implants and the lower jaw were fabricated using 3D printing. 3D printing is a potentially transformative technology in the medical industry that improves clinical practice and surgical education [18]. It helps in maintaining a cordial relationship between surgeons and the patient. Many medical companies are betting on 3D printing to improve product quality and efficiency. There is a wide range of 3D printing techniques that uses a varied range of materials from polymer to metals.

2.2.1. Fabrication of Polymer Model

The Ultra 3SP (Envision TEC, Gladbeck, Germany) polymer 3D printer as shown in Figure 4a was used in the fabrication of the goat lower jaw (Figure 4b). The material used was ABS (acrylonitrile butadiene styrene) plastic in the liquid resin. The Ultra 3SP 3D printer works on the principle of laser-based SLA (Stereolithography) technique where the laser reflects off the mirror and, through a series of optics, focuses the light on the uncured resin and successively solidifies the layers one at a time thereby providing a 2D patterned layer. Ultra 3SP produces parts of high accuracy with a resolution of 100 μm . The polymer models were used to validate the proposed design and assist the surgeon in comprehensive surgical planning, rehearsal, and precision drilling of screws.

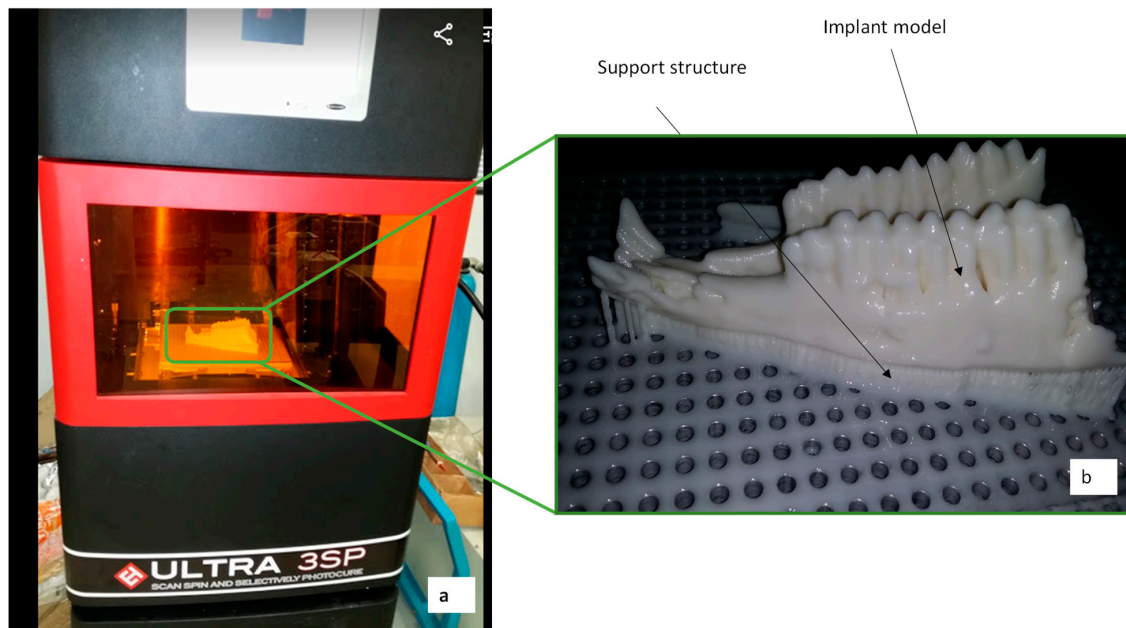


Figure 4. (a) Ultra 3SP 3D printer used for the polymer fabrication of (b) goat mandible.

2.2.2. Fabrication of Titanium Implants

Titanium and its alloys are the most widely used and promising inert material for biomedical applications. Titanium and its alloys form a thin oxide layer film on its surface naturally when exposed to air, which provides excellent biocompatibility and corrosive resistance [19]. The EBM process uses a high-energy beam of electrons to melt the titanium powder (Ti6Al4V ELI). The entire process takes place in a vacuum and at an elevated temperature of 700 °C to reduce the residual stresses and distortion during the build cycle. The working principle of the EBM process can be seen in Hopkins et al. [20], Murr et al. [21], and Heintl et al. [22].

Figure 5 illustrates the EBM-fabricated goat implants with support structures and porous cubes. The support structures were added to remove the dissipated heat from the build and to assist the overhang structures. The time taken for the entire build cycle was approximately 6–8 h. The EBM-built parts were subjected to a powder recovery system (PRS) to remove the semi-sintered powder attached to the build parts. The support structures attached to the implant were easily removed manually with pliers without having any adverse effect on the implants or their parts. The porous cubes were fabricated to study the inner construction of the pore channels. The cubes were designed similar to the pore structure of the goat implant.

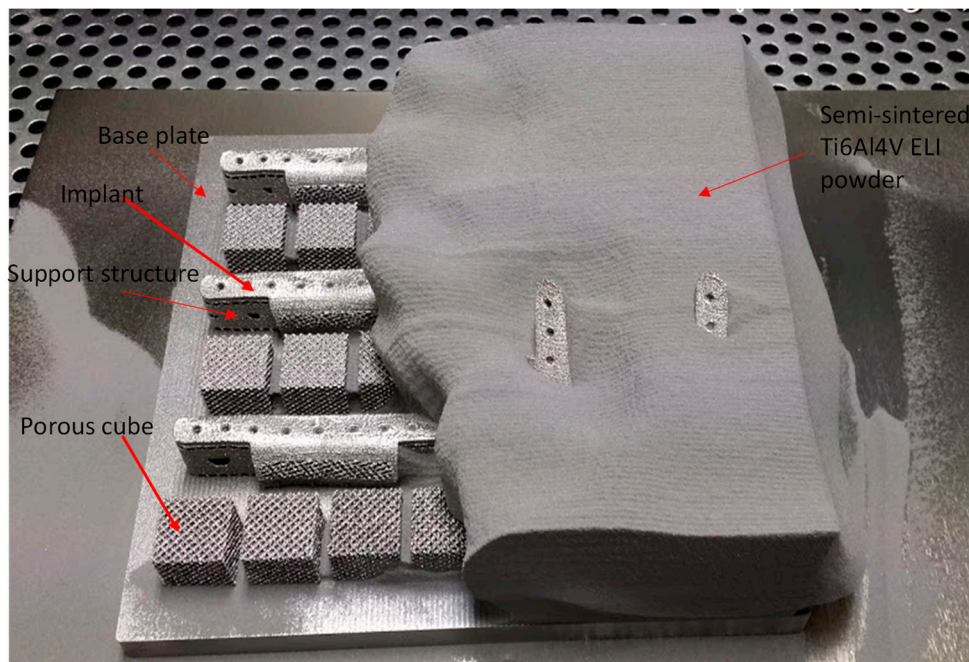


Figure 5. Fabrication of titanium goat implants with dode thick cube structures.

2.3. Implant Evaluation Study

The fabricated EBM implants were investigated for structural analysis, implant fitting, and elemental composition. In addition to these intrinsic tests, a cost analysis was also conducted to examine the EBM production cost of each implant.

2.3.1. Powder Metallurgical Study

EBM is a powder bed fusion process where high energy of heat through beams of electrons was used to melt the Ti6Al4V ELI powder. A powder metallurgical study was conducted to investigate the chemical composition of the material (Ti6Al4V ELI powder) before and after fabrication. Energy Dispersive X-Ray Spectroscopy (EDS) (Oxford instruments, PLC, Abingdon, UK) was used to evaluate the chemical composition of the powder and the EBM specimens.

2.3.2. Pore Structural Analysis

Upon completion of the EBM build, it is a usual practice to blast the semi-sintered powder attached to the build specimen. Blasting is done with a mixture of the same Ti6Al4V ELI powder and highly pressurized air. There are high chances of breakage of the internal pores in the case of porous structures. Pore structural analysis was conducted to analyze the internal connectivity through micro-CT scan analysis. Weak interconnectivity leads to fractures and a good pore channel enhances the implant–tissue ingrowth. A good interconnected pore channel not only offers a corridor for micronutrients but also provides a higher surface area for implant–tissue ingrowth [23]. A solid cube of 15 mm × 15 mm was designed (Figure 6a) and patterned to the porous structure (Figure 6b) using a dode thick cell type of Magics structural module (Materialise, NV, Leuven, Belgium). The dode thick porous structure was then fabricated using the EBM machine as shown in Figure 6c. Bruker Skycam 1173 (Bruker, Billerica, MA, USA) micro-CT scanner was used to visualize the internal defects of the EBM-fabricated porous cube. An accelerating source voltage of 120 kV was used in this study. A high-resolution X-ray beam with a focused spot size of 5 μm was concentrated on the porous cube.

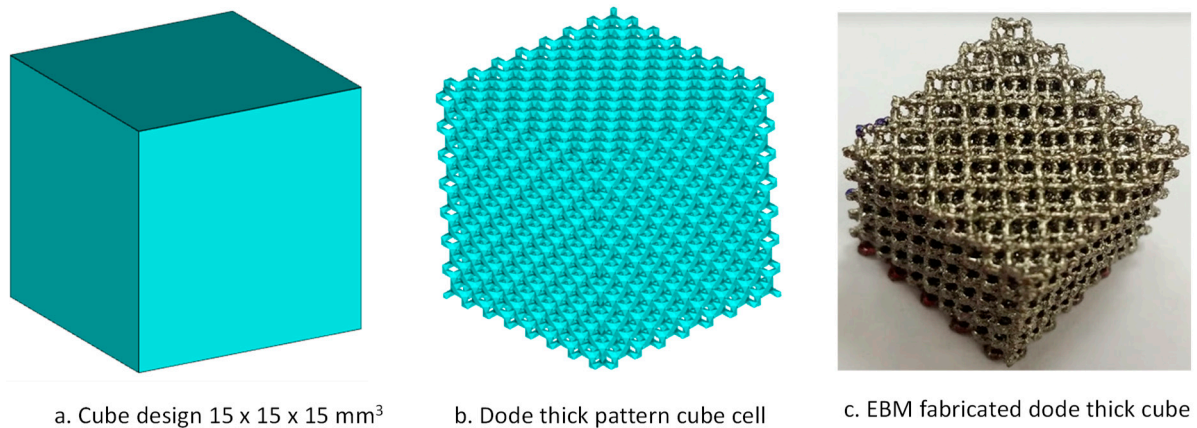


Figure 6. Transformation and fabrication of dode thick cube structure.

2.3.3. Clinical Study

Three study groups of goats were formed for the clinical study of these reconstruction plates. The groupings were done depending on the type of reconstruction plates implanted into the animal to treat the surgical defect. Group 1 was where the mandibular segmental defect was treated with an EBM reconstruction plate with mesh, whereas Group 2 was treated with an EBM reconstruction plate without mesh and Group 3 contained animals with the commercial plate. A total of 15 animals were ear-tagged with numbers and assessed for their oral intake. The weights and physical condition were recorded. The animals were made to fast for 12 h before surgery. General anesthesia (GA) was performed by intramuscular injection of drugs, namely acepromazine (1.5 mg/kg, Vedco, St. Joseph, MO, USA), ketamine (20 mg/kg, Sigma Chemical, St. Louis, MO, USA), and xylazine (5 mg/kg, Lloyd Laboratories, Shenandoah, IA, USA). After GA, the surgical site over the mandible was shaved and disinfected (Figure 7a, and the mandible length was measured from angle to symphysis (Figure 7b). A small linear incision (Figure 7c) was performed on the skin of the lower mandible jaw using a Bard–Parker blade (Size-15). The incision was extended (Figure 7d) to expose the edentulous area in the parasymphysis of the left mandible. An experimental segmental defect was marked and created in this edentulous area (Figure 7e). The reconstruction plates and screws were aligned on the mandibular body region for marking of pilot screw holes. The osteotomy was performed using a small reciprocating saw under saline irrigation (Figure 7f). The segmental bony segment was removed (Figure 7g,h) and the wound was cleaned and irrigated with saline.

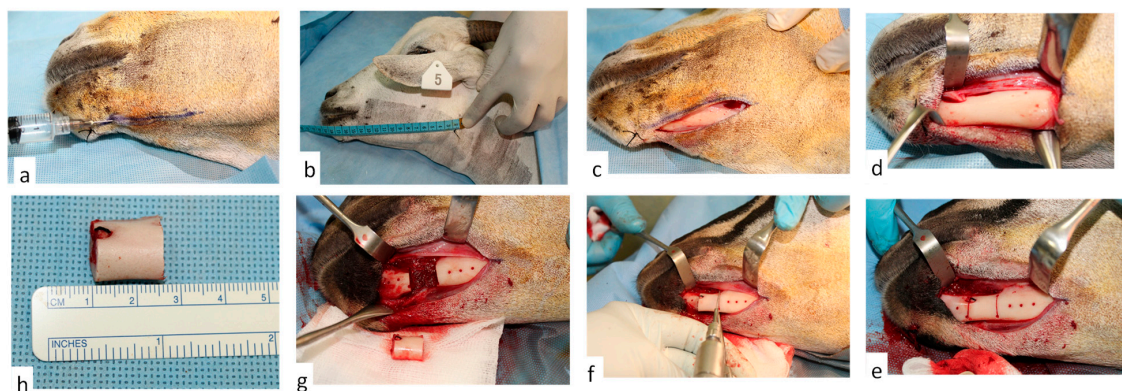


Figure 7. Surgical process: (a) Performing general anesthesia, (b) measuring the mandibular length from angle to symphysis, (c) linear incision was performed, (d) extended the linear incision, (e) marking experimental segmental defect, (f) performing osteotomy using a reciprocating saw, (g) removing the bony segment and (h) measuring the bony segment.

The reconstruction plates were first fixed on the marked segmental margins with screw holes and removed as shown in Figure 8a–c. The three different reconstruction plates were then adopted on the segmental defect and fixed with screws as illustrated in Figure 8d–f. The animals were monitored for signs of infection, pain, and any dysfunctional activities after surgery. They were fed with soft cooked cereals and mineral supplements to nourish healing. Two weeks after surgery, the animals were fed with a conventional cattle diet. Post-operatively, the animals were monitored weekly under veterinary supervision. Post-surgery, the animals were kept at the animal housing facility for the first few weeks, then discharged to the farm. The animal's weight and their oral functionality were assessed to identify any weight loss and their ability to chew food normally. Twelve weeks post-surgery, the goats were sacrificed, and their heads were removed for radio graphical analysis (CBCT) using the protocol mentioned earlier. Following the post-operative CBCT scan, representative hard-tissue and soft-tissue specimens were harvested from the left mandibular segmental defect area adjoining the reconstruction plates. The specimens were fixed for 1 week in 10% neutral buffered formalin and the hard tissue specimens were subsequently decalcified by immersion in 5% formic acid for 8 weeks. All the fixed specimens were embedded in paraffin for preparation of 4 μm thick histological sections, which were stained with hematoxylin and eosin (H & E) stain and subjected to qualitative histological analysis. Histological evaluation was done through a conventional light microscope with facility of digital image capture (ZEISS Axioscope, Berlin, Germany). The qualitative histological examination aimed at identifying the presence or absence of foreign-body inflammatory reaction to the different types of plates, presence of dispersed metal particles, and new bone formation around the plates.

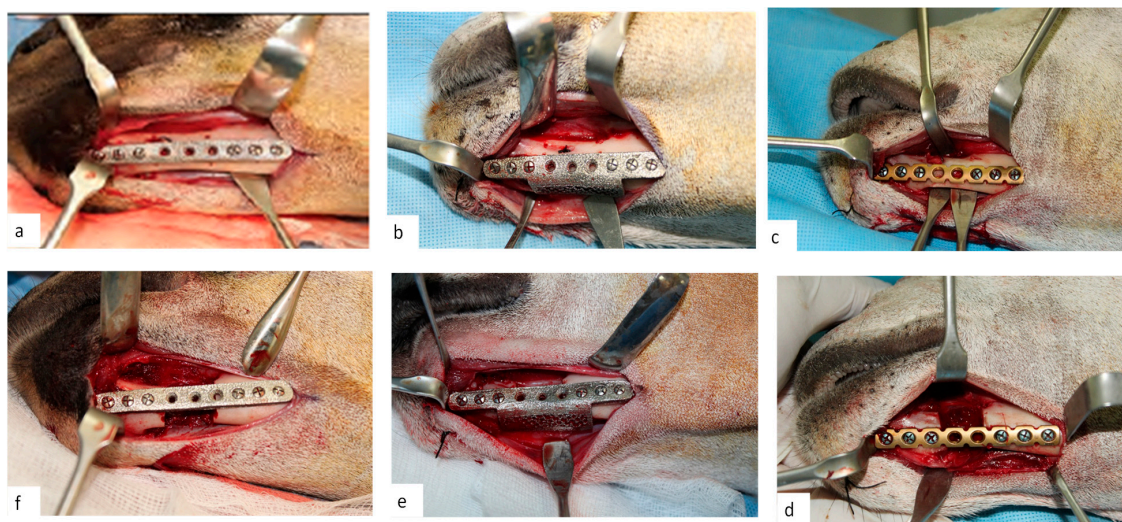


Figure 8. Three different reconstruction plates fixed with screws (d–f) on the previous marked segmental defect margins and screw holes (a–c).

2.3.4. Accuracy Analysis

The different reconstruction plates, including customized EBM plates without mesh, customized EBM plates with mesh, and commercial plates, were investigated for accurate fitting. Accuracy analysis was performed to approximate the gap between the implant and the mandible and to quantify the aesthetics quality and the outer profile of the facial skeleton. Since there are no standard tests available for accuracy evaluation, in this work, a two-stage methodology was adopted to compare and validate the performance of three designs. Initially, all the 15 goats' 3D models obtained from CT scan before surgery were taken as reference data models. In the first stage (pre-operative), the implants in three different groups were analyzed using the Faro Arm scanner and 3D comparison by fitting them on additively fabricated goat mandibles (polymer). The obtained 3D models generated from the Faro Arm scanner were then aligned and superimposed with the reference 3D model to analyze the deviation. In the second stage (post-surgery), the CBCT scans of goat heads were processed and 3D models

were generated using Mimics[®]. The generated 3D models post-surgery were then superimposed on the 3D models of pre-surgery to analyze the deviation. A 3D modeling tool (Geomagics Control 2014, 3D systems, Rock hill, SC, USA) was used to align the data sets and analyze the deviation [24]. The statistical indices employed to measure the accuracy of the implants were the root mean square error (RMSE) and the mean absolute error (MAE) as shown in Equations (1) and (2), respectively. The MAE represents the mean of the absolute values of the individual errors on overall points in the test set (remodeled face with implant). Likewise, the RMSE value (i.e., the square root of the average of squared errors) provides the average magnitude of the error to quantify the overall accuracy for the remodeled goat mandible. These two indices have been used to diagnose and validate the fitting accuracy as well as to determine the variation among the different designs of the implant.

$$\text{RMSE} = \frac{1}{\sqrt{n}} \sqrt{\sum_{i=1}^n (Z_{1,i} - Z_{2,i})^2} \quad (1)$$

$$\text{MAE} = \frac{1}{n} \sum_{i=1}^n |Z_{1,i} - Z_{2,i}| \quad (2)$$

where $Z_{1,i}$ is the reference data set, $Z_{2,i}$ is the test data, and n is the total number of measuring points. The lower the RMS value determined, the better the accuracy found.

First Stage: Faro Arm Scans

The Faro Arm scanning and 3D comparison was employed on the three study groups to quantify the accuracy of the scanned and reconstructed goat implants with a prototype with respect to the reference model before surgery. The 3D comparison analysis was carried out with Geomagics Control software which displays the results by calculating the shortest distance between points on the test model and the respective points on the reference model. The following steps were executed in this stage:

- Acquisition of data: The data for the reconstructed implant mandible models was acquired in the form of the point cloud using a Faro Arm mounted scanner as shown in Figure 9a.
- Distinction of objects as test and reference: The point data for reconstructed implant mandible models from Faro Arm scanner were imported into the software as test models and the original mandible obtained from initial CT scan before surgery was considered to be the reference model.
- Alignment: The imported test mandibular models were aligned and superimposed with the reference mandible models.
- 3D compare: Finally, the surface deviation between the test and the reference mandibular models (Figure 9b–d) were computed. The analysis data of the surface deviation were recorded.

Second Stage: CBCT Scans

A CBCT scan was performed in the second stage on all the animals after 12 weeks post-surgery. The CBCT scan images were then converted into 3D models using Mimics[®] (Figure 10a orange) and their accuracy was assessed in comparison to the pre-surgery 3D models (Figure 10a Blue) using 3D comparison as shown in Figure 10b.

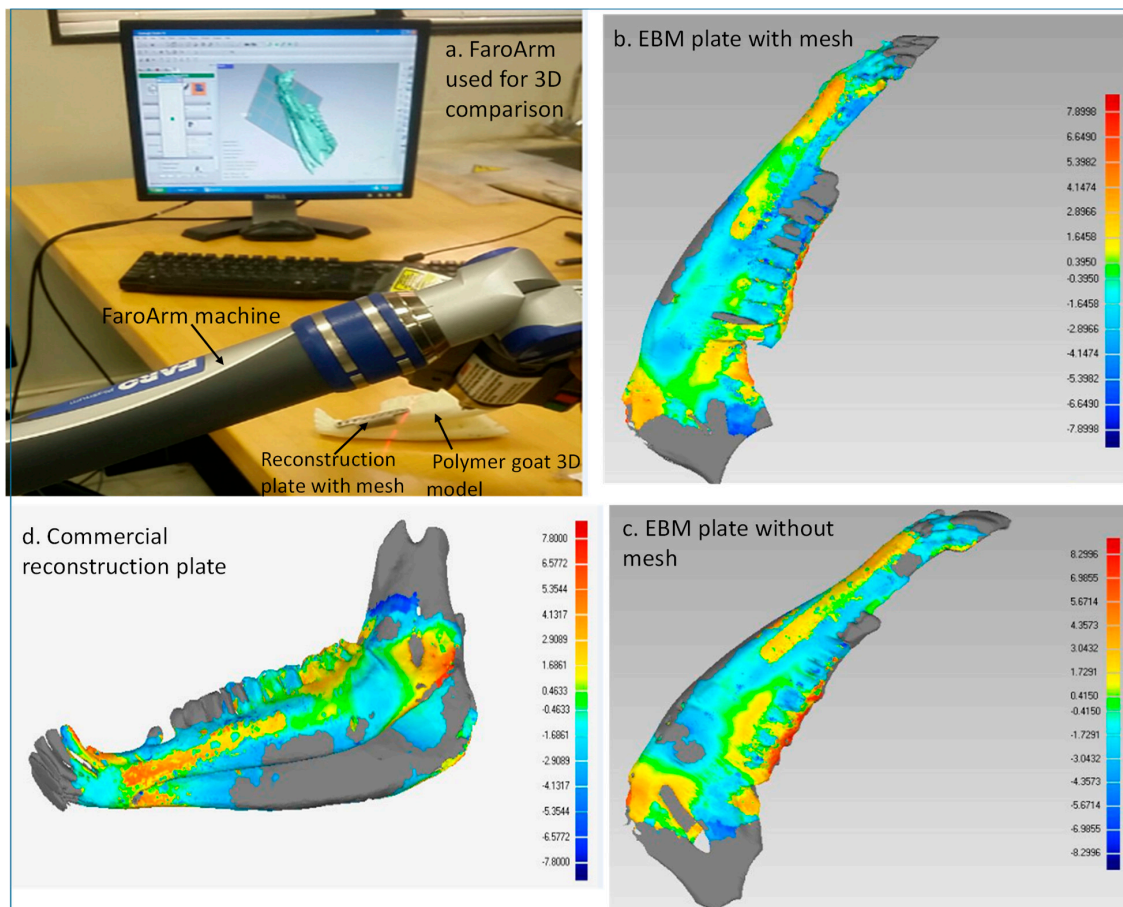


Figure 9. 3D comparison results for three reconstruction plates using Faro Arm.

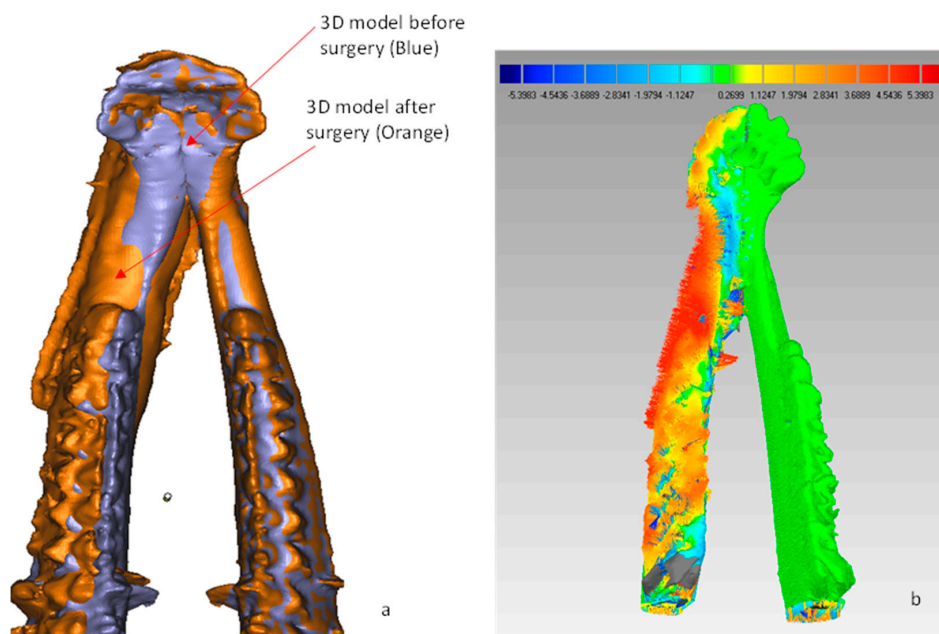


Figure 10. (a) The alignment of 3D models before and after surgery and (b) the computed surface deviation test results of a reconstruction mesh plate.

2.3.5. Cost Analysis

The economics of EBM production of reconstruction plates has also been examined. As EBM works on the additive manufacturing principle, less material is used which results in the reduction of material cost and manufacturing time [25]. One of the main cost-driving factors in the implant production cost is the EBM machine run time. Multiple parts can be produced in a single EBM build cycle. In addition to the benefits of cost, energy, and sustainability, AM properties, and performance are important factors in assessing the suitability of this technology. Studies have proved that EBM technology can produce parts with properties exceeding those manufactured by traditional processes [26]. The cost model for the EBM-produced parts are defined as follows:

$$\text{Cost Model } C_{Build} = [(C_{Indirect} \times T_{Build}) + (M_{Part} \times C_{Raw}) + (E_{Build} \times C_{Energy}) + (M_{Hours} \times C_{Labor})]$$

where

$C_{Indirect}$ —Indirect cost comprising EBM ownership cost and maintenance cost, measured in \$/h,

T_{Build} —EBM total build time,

M_{Part} —Mass of EBM-built parts including support structures,

C_{Raw} —Cost of the raw material (Ti6Al4V ELI) measured in \$/g,

E_{Build} —Energy consumption for EBM-built part,

C_{Energy} —Energy consumption cost (Electricity cost for EBM process), measured in \$/KWh.

M_{Hours} —Manual hours spend in preparing the EBM build parts,

C_{Labor} —Cost of the labor/HR

3. Results

The EDS results as illustrated in Figure 11 and Table 1 concluded that there was not any significant difference in the chemical composition of the Ti6Al4V ELI material upon the heat source.

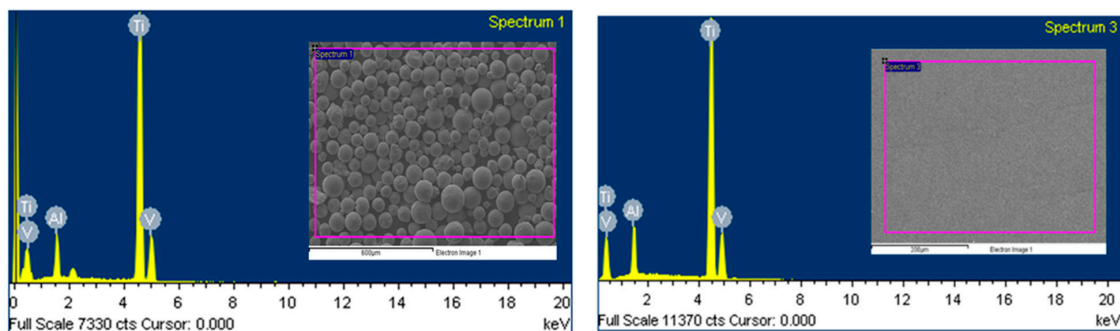


Figure 11. Chemical composition of the Ti6Al4V ELI feedstock powder (left) and EBM-fabricated specimen (right) obtained through EDS Test.

Table 1. Chemical specifications of the ASTM Standards, feedstock powder and EBM-fabricated specimen (wt. %) of Ti6Al4V ELI material.

Chemical Specification (wt. %)	Al (Aluminum)	V (Vanadium)	Ti (Titanium)
ASTM [F136] standards [27]	5.5–6.5	3.5–4.5	88–91
Feedstock powder	6.4	4.0	89.6
EBM Fabrication Specimen	6.24	3.89	89.87

The metallurgical results also indicated that the EBM-fabricated surface met the ASTM standards and was ideal for osseointegration in promoting bone-ingrowth. The micro-CT scan results as illustrated in Figure 12 revealed the internal architecture of the porous cube of dode thick unit cell. It confirmed that the EBM-fabricated porous cube was finely interconnected by a series of channels and free from

any cracks and internal defects such as voids. As a result, a similar kind of interconnectivity of pores was assumed for the porous goat implant with a dodecahedral structure.

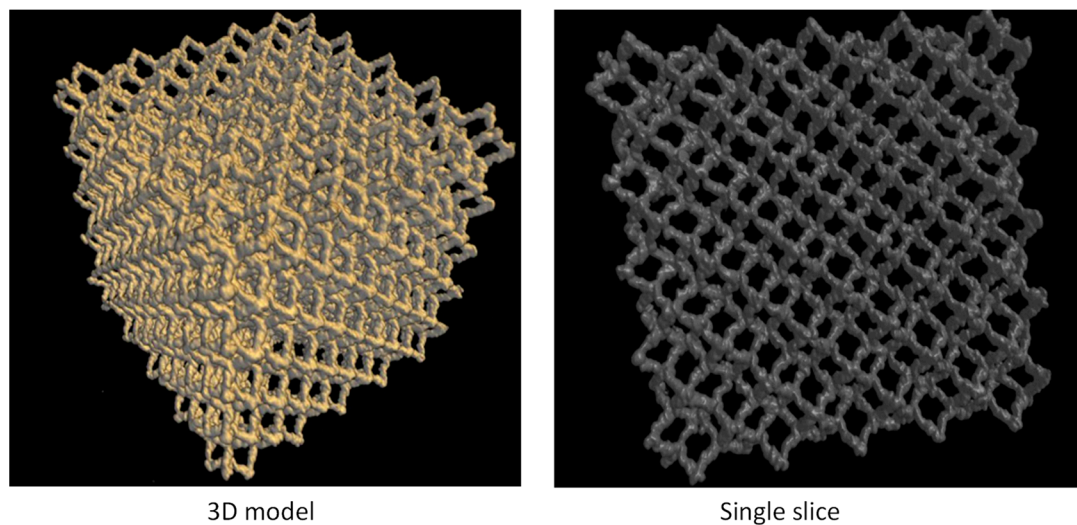


Figure 12. Micro-CT scan of dodecahedral thick cube for checking internal defects.

The histological study on post-operative specimens obtained from the goat mandibles revealed new bone formation with osteoblast cell attachment and proliferation on the EBM reconstruction plates and the commercial plate. Mild inflammatory reaction and mixed micrometer particles of titanium were observed in the hard tissue and soft tissue specimens obtained from animals in all the three groups (Figure 13a). However, no clinically discernible foreign-body reaction took place in any of these animals during the entire post-operative study period. The inflammatory response in the tissues could also be attributed to the physiological healing mechanism of the long-term study. Nevertheless, newly formed cancellous bone islands with osteocytes and neovascularization interspersed with connecting tissue was seen at the defect site adjoining the reconstruction plates in all the animals as shown histologically in Figure 13b. While no quantitative estimation was done, the amount of new bone formation was clearly higher in the segmental defects reconstructed using the EBM titanium reconstruction plate with mesh design, than with the other types.

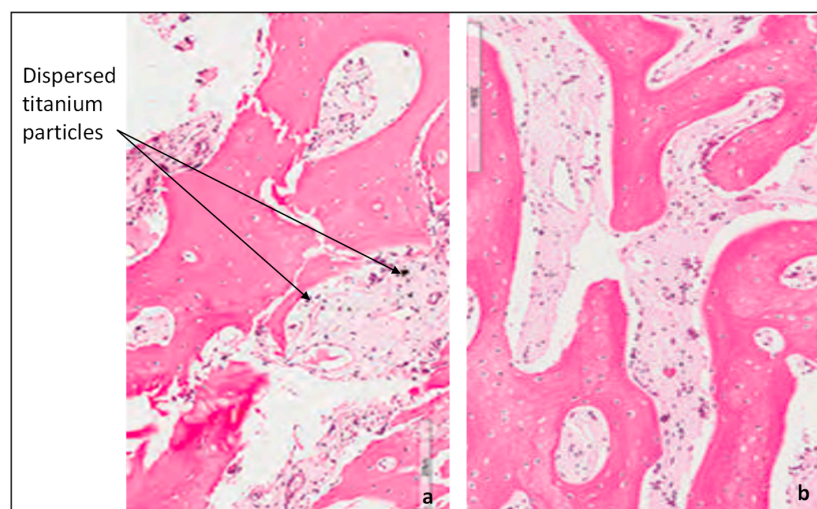


Figure 13. Histological analysis of specimens showing (a) mild inflammatory and sub-micrometer particles of dispersed material within the bone and (b) islands of newly formed cancellous bone and neovascularization interspersed with the connecting tissue.

The outcome from the first-stage analysis revealed that the customized plate with mesh had the highest accuracy (RMS 2.5270 mm and MAE 1.951 mm), while the commercial plate provided the lowest accuracy (RMS 2.6692 mm and MAE 2.149 mm). The customized plate without mesh (RMS 2.6545 mm and 2.118 mm) provided relatively better performance as compared to the commercial plate.

The outcome from the second-stage analysis also revealed that the customized plate with mesh had the highest accuracy (RMS 2.0616 mm and MAE 1.362 mm), while the commercial plate provided the lowest accuracy (RMS 2.288 mm and 1.593 mm). The customized plate without mesh (RMS 2.2696 mm and MAE 1.461 mm) provided relatively better performance as compared to the commercial plate. The agreement of results as shown in Table 2 for the two stages validates the accuracy of the different implant designs. The lower accuracy of different plates at the second stage suggests that the plates adapted themselves within the body after surgery. Moreover, it can also be inferred that the commercial plate and the customized plate without mesh performed quite similarly in terms of fitting accuracy. It means that the mesh had a role in enhancing the fitting accuracy of the implant.

Table 2. 3D comparison results data of the study animals from different groups.

Study Group	RMS (mm)		MAE (mm)	
	First Stage	Second Stage	First Stage	Second Stage
Group-1 (EBM titanium reconstruction plate with mesh)	2.5270	2.0616	1.951	1.362
Group-2 (EBM titanium reconstruction plate without mesh)	2.6545	2.2696	2.118	1.461
Group-3 (Commercial reconstruction plate)	2.6692	2.2880	2.149	1.593

The results of the EBM reconstruction plate cost were compared with the commercially available reconstruction plates. Table ST1 (attached in the supplementary file) represents the comprehensive spreadsheet of cost estimates for producing the EBM reconstruction plates with mesh and without mesh. It was observed from the cost analysis results that the EBM production cost of a single reconstruction plate was in the range of \$46–\$52, which was significantly less than the cost of commercial plates (\$250–\$330) [28].

4. Discussion

EBM technology has proven to be an excellent choice for medical implants. Parts produced through the EBM process are much faster when compared to traditional means. Moreover, parts produced through EBM can have much better control over their internal and external structures. Palmquist et al. [29] evaluated the EBM-fabricated cylindrical discs implanted in sheep femur and dorsum. Thomsen et al. [30] examined the EBM-produced titanium discs with 29% to 41% bone-in-implant contact over 6 weeks in rabbits. EBM-produced titanium (Ti6Al4V ELI) parts have previously been implanted in several animal and human studies [15,16]. However, very few studies have been reported in the customization and in vivo clinical assessment of mesh implants. This study is directed to investigate the effects of customized mesh plate in comparison with the customized bulk plate and commercial plate without mesh using an in vivo study on goats. In addition to clinical assessment, pre- and post-radiographic analysis was performed to evaluate the efficacy of reconstruction plates towards anatomical and physiological functions.

The present study demonstrates the digital workflow from the CT scan, conversion of raw data to 3D models, implant customization, and clinical performance of mandibular reconstruction plates. The computer-aided design and virtual pre-operative surgical planning of customized reconstruction plates with polymer models improves the implant–bone contact area, reduces the operating time, and leads to better surgery outcomes [31]. Moreover, operation cost savings result from the reduction of time in pre-bending of plates and pre-operative surgical planning with polymer models [32]. However,

in the case of commercial plates, additional time is needed in surgical planning and bending of plates which would result in increased cost for the surgery.

The study demonstrates the evaluation of the accuracy of the reconstruction plates on post-operation. The maxilla-mandibular occlusion was found to be stable throughout the study, thus signifying the anatomical and functional stability of the implanted EBM reconstruction plates. At 18 weeks post-operation, all the study animals were performing their oral functions effectively without any hindrance or adverse biological reaction in any of the reconstruction plates. The chewing patterns of the goats were normal, while a slight reduction in weight of less than 1 kg was observed after 3 months. This could be due to the reduction of oral intake because of reconstruction plates or due to the housing of goats in an isolated facility (animal housing facility at the university). The segmental defects healed properly without any dehiscence and no significant difference was observed in the pre-operative and post-operative clinical parameters. Figure 14 illustrates the healed segmental defect of three different reconstruction plates with arrows indicating the bone-healing and filling of defects.

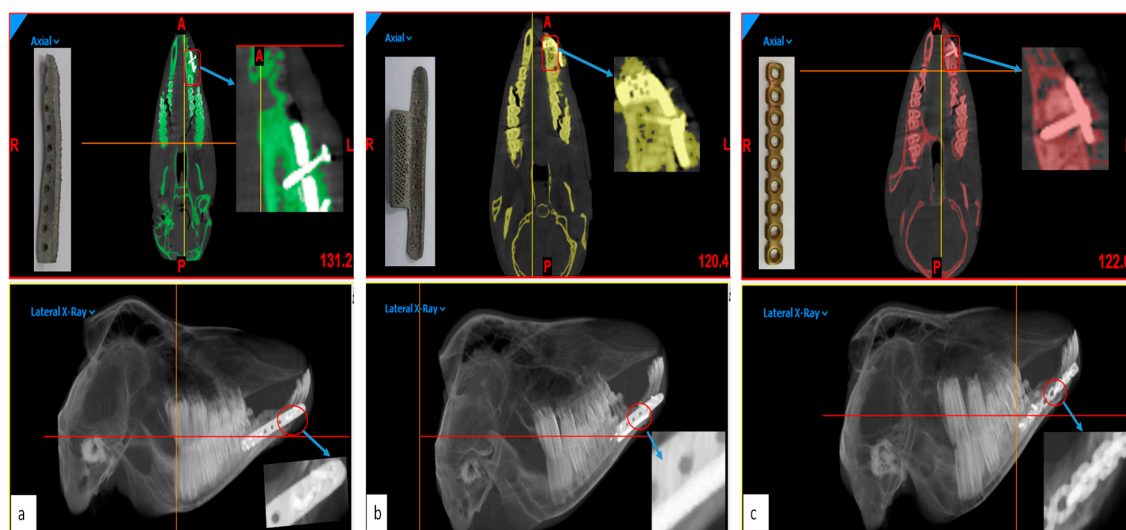


Figure 14. The healed segmental defects of three different goats with (a) reconstruction plate without mesh, (b) reconstruction plate with mesh and (c) synthesis commercial plate after 3 months post-surgery (arrows indicating the titanium plates filling the defects).

Cost analysis results illustrates that the EBM-produced direct custom-built plates are cost efficient when compared to commercially available reconstruction plates. As EBM can produce many parts in a single build, the EBM production cost can be reduced by increasing the implant quantity. Simultaneously, the EBM would be an expensive process when producing a single implant as compared to the commercial plate. Furthermore, the commercially available reconstruction plates are not customized, unlike EBM reconstruction plates, which are custom-built. These commercial plates are straight in design and would require manual bending before or during surgery to custom fit a curved jaw. The surgeons spent a considerable amount of time (1–2 h) trying to bend the plate as per the patient's bone contours. Moreover, the commercial plates are produced through traditional techniques such as casting [33] and wrought technique [34], which is an expensive process

5. Conclusions

The advent of image-processing techniques and additive manufacturing has been creating significant opportunities in the customization of mandibular reconstruction implants. Therefore, the objective of this study was comparing the performance of EBM-fabricated customized plates with and without mesh with that of the commercial plate. Two sets of customized reconstruction plates, one with mesh and other without mesh, were fabricated using EBM and the third set of commercial plates was manually bent and embedded inside the goat to study biocompatibility and implant accuracy.

Animal results indicated that the EBM-fabricated mesh plate provided superior results statistically. Therefore, it can be concluded that EBM-fabricated mesh plates with interconnected channels of pores are one of the main prerequisites for bone–tissue formation and subsequent biomechanical anchorage. It has also proved that the EBM-fabricated mesh plate is a practical alternative to commercial plates with its superior biocompatibility and implant fitting accuracy.

Supplementary Materials: The following are available online at <http://www.mdpi.com/2075-4701/9/10/1065/s1>, Table ST1: Implant cost calculation spreadsheet for Electron beam melting, Table ST2: Price calculation of major EBM spare parts (Consumables).

Author Contributions: K.M. conceived and designed the experiments; K.M. & S.H.M. performed the experiments; S.R. and M.A. performed the clinical study; H.A. and O.A. analyzed the data; K.M. & S.H.M. wrote and reviewed the paper.

Funding: This research was funded by Deanship of Scientific Research, King Saud University: Research group no. RG-1440-075.

Acknowledgments: The authors extend their appreciation to the Deanship of Scientific Research at King Saud University for funding this work through research group no (RG-1440-075).

Conflicts of Interest: The authors have no conflict of interest to declare.

Ethical Statement: Ethical committee at the College of Dentistry Research Center, King Saud University, Riyadh, Saudi Arabia (Registration # PR-0034).

References

1. Maurer, P.; Eckert, A.W.; Kriwalsky, M.S.; Schubert, J. Scope and limitations of methods of mandibular reconstruction: a long-term follow-up. *Br. J. Oral Maxillofac. Surg.* **2010**, *48*, 100–104. [[CrossRef](#)] [[PubMed](#)]
2. Khorasani, A.M.; Goldberg, M.; Doeven, E.H.; Littlefair, G. Titanium in Biomedical Applications-Properties and Fabrication: A Review. *J. Biomater. Tissue Eng.* **2015**, *5*, 593–619. [[CrossRef](#)]
3. Moiduddin, K.; Darwish, S.; Al-Ahmari, A.; ElWatidy, S.; Mohammad, A.; Ameen, W. Structural and mechanical characterization of custom design cranial implant created using additive manufacturing. *Electron. J. Biotechnol.* **2017**, *29*, 22–31. [[CrossRef](#)]
4. Parthasarathy, J. 3D modeling, custom implants and its future perspectives in craniofacial surgery. *Ann. Maxillofac. Surg.* **2014**, *4*, 9–18. [[CrossRef](#)] [[PubMed](#)]
5. Ryan, G.; Pandit, A.; Apatsidis, D. Fabrication methods of porous metals for use in orthopaedic applications. *Biomaterials* **2006**, *27*, 2651–2670. [[CrossRef](#)] [[PubMed](#)]
6. Wang, X.; Xu, S.; Zhou, S.; Xu, W.; Leary, M.; Choong, P.; Qian, M.; Brandt, M.; Xie, Y.M. Topological design and additive manufacturing of porous metals for bone scaffolds and orthopaedic implants: A review. *Biomaterials* **2016**, *83*, 127–141. [[CrossRef](#)]
7. Ângelo, D.F.; Morouço, P.; Alves, N.; Viana, T.; Santos, F.; González, R.; Monje, F.; Macias, D.; Carrapiço, B.; Sousa, R.; et al. Choosing sheep (*Ovis aries*) as animal model for temporomandibular joint research: Morphological, histological and biomechanical characterization of the joint disc. *Morphologie* **2016**, *100*, 223–233. [[CrossRef](#)] [[PubMed](#)]
8. Pal, T.K.; Chakraborty, A.; Banerjee, S. A micro-anatomical comparison of goat jaw cancellous bone with human mandible: Histomorphometric study for implant dentistry. *J. Int. Clin. Dent. Res. Organ.* **2014**, *6*, 20–23.
9. Martola, M.; Lindqvist, C.; Hänninen, H.; Al-Sukhun, J. Fracture of titanium plates used for mandibular reconstruction following ablative tumor surgery. *J. Biomed. Mater. Res. B Appl. Biomater.* **2007**, *80*, 345–352. [[CrossRef](#)]
10. Yang, W.F.; Choi, W.S.; Leung, Y.Y.; Curtin, J.P.; Du, R.; Zhang, C.Y.; Chen, X.S.; Su, Y.X. Three-dimensional printing of patient-specific surgical plates in head and neck reconstruction: A prospective pilot study. *Oral Oncol.* **2018**, *78*, 31–36. [[CrossRef](#)]
11. Xilloc/Patient Specific Implants, Mandible Reconstruction Plate: Patient-Specific and 3D Printed. 27 August 2014. Available online: https://www.xilloc.com/products_services/mandible_recon/ (accessed on 21 May 2019).

12. Ayoub, N.; Ghassemi, A.; Rana, M.; Gerressen, M.; Riediger, D.; Hölzle, F.; Modabber, A. Evaluation of computer-assisted mandibular reconstruction with vascularized iliac crest bone graft compared to conventional surgery: A randomized prospective clinical trial. *Trials* **2014**, *15*, 114. [CrossRef] [PubMed]
13. Bertollo, N.; da Assuncao, R.; Hancock, N.J.; Lau, A.; Walsh, W.R. Influence of Electron Beam Melting Manufactured Implants on Ingrowth and Shear Strength in an Ovine Model. *J. Arthroplast.* **2012**, *27*, 1429–1436. [CrossRef] [PubMed]
14. Cronskär, M.; Rännar, L.E.; Bäckström, M. Implementation of Digital Design and Solid Free-Form Fabrication for Customization of Implants in Trauma Orthopaedics. *J. Med. Biol. Eng.* **2012**, *32*, 91. [CrossRef]
15. Lethaus, B.; ter Laak, M.P.; Laeven, P.; Beerens, M.; Koper, D.; Poukens, J.; Kessler, P. A treatment algorithm for patients with large skull bone defects and first results. *J. Cranio-Maxillofac. Surg.* **2011**, *39*, 435–440. [CrossRef]
16. Suska, F.; Kjeller, G.; Tarnow, P.; Hryha, E.; Nyborg, L.; Snis, A.; Palmquist, A. Electron Beam Melting Manufacturing Technology for Individually Manufactured Jaw Prosthesis: A Case Report. *J. Oral Maxillofac. Surg.* **2016**, *74*, 1706.e1–1706.e15. [CrossRef] [PubMed]
17. Zhang, J.; Jung, Y.-G. *Additive Manufacturing: Materials, Processes, Quantifications and Applications*; Elsevier: Amsterdam, The Netherlands, 2018; ISBN 978-0-12-812155-9.
18. Jones, D.B.; Sung, R.; Weinberg, C.; Korelitz, T.; Andrews, R. Three-Dimensional Modeling May Improve Surgical Education and Clinical Practice. *Surg. Innov.* **2016**, *23*, 189–195.
19. De Viteri, V.S.; Fuentes, E. Titanium and Titanium Alloys as Biomaterials. In *Tribology-Fundamentals and Advancements*; IntechOpen: Rijeka, Croatia, 2013; pp. 155–181.
20. Hopkinson, N.; Dickens, P. Emerging Rapid Manufacturing Processes. In *Rapid Manufacturing*; John Wiley & Sons, Ltd.: Hoboken, NJ, USA, 2006; pp. 55–80.
21. Murr, L.; Esquivel, E.; Quinones, S.; Gaytan, S.; López, M.; Martínez, E.; Medina, F.; Hernandez, D.; Martínez, E.; Martínez, J.; et al. Microstructures and mechanical properties of electron beam-rapid manufactured Ti–6Al–4V biomedical prototypes compared to wrought Ti–6Al–4V. *Mater. Charact.* **2009**, *60*, 96–105. [CrossRef]
22. Heintz, P.; Korner, C.; Singer, R.F. Selective Electron Beam Melting of Cellular Titanium: Mechanical Properties. *Adv. Eng. Mater.* **2008**, *10*, 882–888. [CrossRef]
23. Vishwakarma, A.; Karp, J.M. *Biology and Engineering of Stem Cell Niches*; Academic Press: Cambridge, MA, USA, 2017.
24. Luthardt, R.G.; Koch, R.; Rudolph, H.; Walter, M.H. Qualitative computer aided evaluation of dental impressions in vivo. *Dent. Mater.* **2006**, *22*, 69–76. [CrossRef]
25. Geraedts, J.; Doubrovski, E.; Verlinden, J. Three Views on Additive Manufacturing: Business, Research, and Education. In Proceedings of the Tools and Methods of Competitive Engineering, Karlsruhe, Germany, 7–11 May 2012; Horváth, I., Albers, A., Behrendt, M., Rusák, Z., Eds.; Delft University of Technology: Delft, The Netherlands, 2012.
26. Facchini, L.; Magalini, E.; Robotti, P.; Molinari, A. Microstructure and mechanical properties of Ti-6Al-4V produced by electron beam melting of pre-alloyed powders. *Rapid Prototyp. J.* **2009**, *15*, 171–178. [CrossRef]
27. Arcam EBM system, Ti6Al4V ELI Titanium Alloy. 14 January 2014. Available online: <http://www.arcam.com/wp-content/uploads/Arcam-Ti6Al4V-ELI-Titanium-Alloy.pdf> (accessed on 3 June 2019).
28. Rustemeyer, J.; Melenberg, A.; Sari-Rieger, A. Costs incurred by applying computer-aided design/computer-aided manufacturing techniques for the reconstruction of maxillofacial defects. *J. Craniomaxillofac. Surg.* **2014**, *42*, 2049–2055. [CrossRef] [PubMed]
29. Palmquist, A.; Snis, A.; Emanuelsson, L.; Browne, M.; Thomsen, P. Long-term biocompatibility and osseointegration of electron beam melted, free-form-fabricated solid and porous titanium alloy: Experimental studies in sheep. *J. Biomater. Appl.* **2013**, *27*, 1003–1016. [CrossRef] [PubMed]
30. Thomsen, P.; Malmström, J.; Emanuelsson, L.; Rene, M.; Snis, A. Electron beam-melted, free-form-fabricated titanium alloy implants: Material surface characterization and early bone response in rabbits. *J. Biomed. Mater. Res. B Appl. Biomater.* **2009**, *90*, 35–44. [CrossRef] [PubMed]
31. Metzler, P.; Geiger, E.J.; Alcon, A.; Ma, X.; Steinbacher, D.M. Three-dimensional virtual surgery accuracy for free fibula mandibular reconstruction: planned versus actual results. *J. Oral Maxillofac. Surg.* **2014**, *72*, 2601–2612. [CrossRef] [PubMed]

32. Xia, J.J.; Phillips, C.V.; Gateno, J.; Teichgraeber, J.F.; Christensen, A.M.; Gliddon, M.J.; Lemoine, J.J.; Liebschner, M.A. Cost-Effectiveness Analysis for Computer-Aided Surgical Simulation in Complex Cranio-Maxillofacial Surgery. *J. Oral Maxillofac. Surg.* **2006**, *64*, 1780–1784. [[CrossRef](#)] [[PubMed](#)]
33. Joshi, A.M. Process planning for the rapid machining of custom bone implants. Master's Thesis, Iowa State University, Ames, IA, USA, 2011.
34. Fazel, R. *Biomedical Engineering—from Theory to Applications*; InTechOpen: Rijeka, Croatia, 2011.



© 2019 by the authors. Licensee MDPI, Basel, Switzerland. This article is an open access article distributed under the terms and conditions of the Creative Commons Attribution (CC BY) license (<http://creativecommons.org/licenses/by/4.0/>).